energies

MDPI

Article

A Variable Fractional Order Fuzzy Logic Control Based MPPT Technique for Improving Energy Conversion Efficiency of Thermoelectric Power Generator

N. Kanagaraj [1,*], Hegazy Rezk [1,2] and Mohamed R. Gomaa [3,4]

1 Electrical Engineering Department, College of Engineering at Wadi Aldawaser, Prince Sattam Bin Abdulaziz University, Al-Kharj 11991, Saudi Arabia; hr.hussien@psau.edu.sa
2 Electrical Engineering Department, Faculty of Engineering, Minia University, Al Minya 61519, Egypt
3 Mechanical Engineering Department, Benha Faculty of Engineering, Benha University, Benha 13512, Egypt; behiri@bhit.bu.edu.eg
4 Mechanical Engineering Department, Faculty of Engineering, Al-Hussein Bin Talal University, Ma'an 71111, Jordan
* Correspondence: k.gonder@psau.edu.sa

Received: 23 July 2020; Accepted: 30 August 2020; Published: 1 September 2020

Abstract: Thermoelectric generation technology is considered to be one of the viable methods to convert waste heat energy directly into electricity. The utilization of this technology has been impeded due to low energy conversion efficiency. This paper aims to improve the energy conversion efficiency of the thermoelectric generator (TEG) model with a novel maximum power point tracking (MPPT) technique. A variable fractional order fuzzy logic controller (VFOFLC)-based MPPT technique is proposed in the present work in which the operating point of the TEG is moved quickly towards an optimal position to increase the energy harvesting. The fraction order term α, introduced in the MPPT algorithm, will expand or contract the input domain of the fuzzy logic controller (FLC to shorten the tracking time and maintain a steady-state output around the maximum power point (MPP). The performance of the proposed MPPT technique was verified with the TEG model by simulation using MATLAB /SIMULINK software. Then, the overall performance of the VFOFLC-based MPPT technique was analyzed and compared with Perturb and observe (P&O) and incremental resistance (INR)-based MPPT techniques. The obtained results confirm that the proposed MPPT technique can improve the energy conversion efficiency of the TEG by harvesting the maximum power within a shorter time and maintaining a steady-state output when compared to other techniques.

Keywords: waste heat recovery; renewable energy; thermoelectric generator; MPPT; fuzzy logic control; fractional order control; energy efficiency

1. Introduction

Recently, research on the alternative method of generating electricity has increased significantly due to environmental issues and the rising electricity demand. Presently, conventional sources are the major sources for electricity generation in most of the countries that lead to various environmental-related issues. The use of fossil fuel, for instance, results in global warming and emission of greenhouse gases, which causes the diminution of the ozone layer. Thus, the utilization of alternative sources for electric power generation has a higher priority nowadays around the world. Among the various alternative sources, the power generation from renewable energy sources has attracted more attention in recent years. Thermoelectric generator (TEG) is one that has emerged

as a better alternative source for electric power generation and successful implementation has been reported in the latest literature. TEGs work via Seebeck's effect, by which the thermal energy is directly converted into electricity. The energy conversion in TEG is usually made by the combination of a thermoelectric module (TEM) and a converter circuit, the TEM converts the heat flux directly into electricity and the converter circuit is used to amplify the output power [1]. When compared to the conventional energy sources, TEGs can be operated with low-grade thermal energy and solar thermal energy; these sources provide costless heat and are efficient. In TEG technology, even a small difference in temperature between hot-end and cold-end can provide enough electricity for low-power electronic appliances. For example, the system-on-chips (SoC) [2], wireless sensors [3,4], and autonomous multisensory systems [5] have been successfully powered by TEGs.

Because of the low energy conversion efficiency, TEGs were not widely used for electric power generation in the past [6]. The energy conversion efficiency of the TEG is typically around 5–10%. Further, this technology has been impeded because of the inconsistent output due to temperature variations. To improve the thermal and electrical performance of TEGs, a lot of research has been done in various aspects such as load resistance [7,8], contact resistance [9], geometry configuration [10–13], sandwiched planner structure [14], improving electro-thermal couple effect [15–18], and so on. TEGs are usually made up of several thermoelectric elements (TEEs), which are connected in series and parallel in an array form to generate the required voltage and current. The equivalent circuit of the TEG can be represented with a simple circuit consisting of a DC voltage source connected in series with internal resistance. According to the principle of maximum power transfer, if the internal resistance of the TEG is equal to the load resistance, then it will deliver the maximum power. Based on the principle of maximum power transfer, several maximum power point tracking (MPPT) algorithms [19–22] have been implemented with different control logic to harvest the maximum power from the TEG. The MPPT techniques are generally used for the TEG system to move its operating point towards the optimal point in the I-V curve corresponding to maximum power. Consider that if a TEG is connected directly to the load, the load impedance will set the operating point, which results in the TEG output being less than the maximum power [6].

The MPPT technique is considered to be an efficient mechanism to improve the performance of the TEG. To improve the efficiency of the renewable energy system by extracting the maximum power, several MPPT techniques have been applied: artificial neural networks (ANN) [23], fractional open-circuit voltage [6], fuzzy logic control [24], a microcomputer with look-up table [25], perturb and observe method (P&O) [26,27], incremental impedance and incremental conductance method (INC) [28], internal resistance method [29], and the hill climbing (HC) technique [30]. These techniques are widely used because of their simple logic and ease of implementation. In this paper, a novel variable fractional order fuzzy logic controller (VFOFLC)-based MPPT scheme is proposed to enhance the energy conversion efficiency of the TEG. The variable tracking step size is applied in the present MPPT scheme using a dynamic variable fractional factor whose value is calculated based on the voltage output of the TEG. The results of the present MPPT tracker are analyzed and compared with the P&O and incremental resistance (INR)-based trackers.

The subsequent parts of this paper are arranged as follows: Section 2 presents the modeling of the thermoelectric generator and its validation. The incremental conduction resistance-based MPPT technique is discussed in Section 3. Section 4 describes the VFOFLC-based MPPT technique. The implementation of the VFOFLC-based MPPT technique is explained in Section 5. In Section 6, the study results are analyzed and discussed. The findings of this research are given in Section 7 as conclusions.

2. TEG Model

2.1. Modeling of the Thermoelectric Generator

TEGs are generally designed with thermocouples; each thermocouple consists of p-type and n-type pellets. Thermocouples are connected in parallel to decrease its thermal resistance and connected in series to increase the electromotive force (e.m.f). The thermocouples are inserted between two ceramic heat exchanger plates; hot-side and cold-side as shown in Figure 1. When a temperature difference is sustained between the two sides, the thermal excitation makes the moment of charger carriers from the hot-end to cold-end, thus a Thompson e.m.f is developed [31,32]. At the same time, there exists a difference in the concentration charge carrier between the thermocouple, which creates a Peltier e.m.f. The complete TEG can be represented with a simple electrical equivalent circuit with a DC voltage source (V_s), an internal resistance (R_{int}), and load resistance (R_L) as seen in Figure 2.

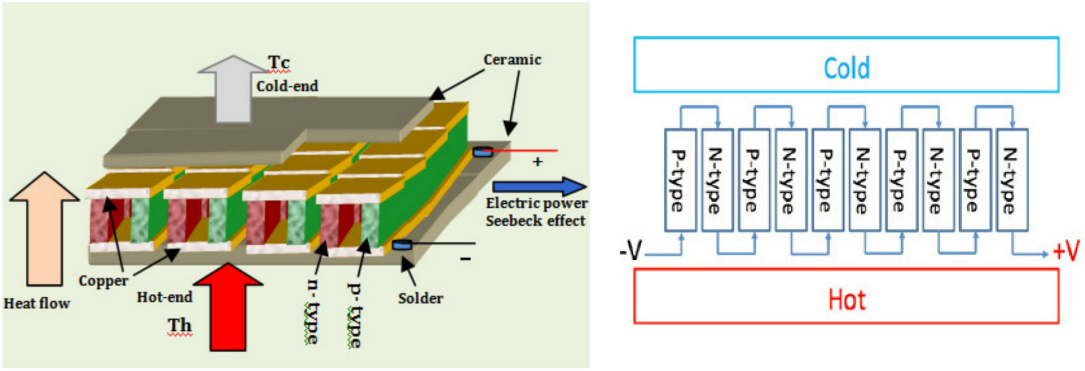

(**a**) (**b**)

Figure 1. (**a**) Model of a thermoelectric generator (TEG) showing the details (**b**) schematic diagram of thermoelectric couples in a TEG.

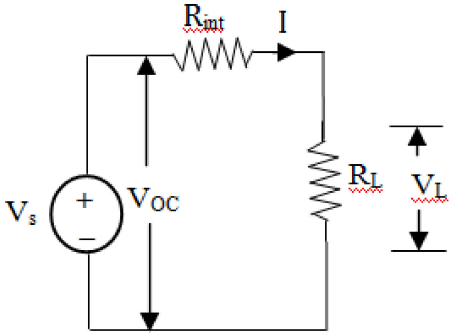

Figure 2. TEG electrical equivalent circuit.

The Seebeck effect, which is the base of TEG, states that an e.m.f is generated between two conductive materials when a temperature difference exists [33]. The generated open-circuit voltage (V_{OC}) of a TEG can be determined using the following Equation (1)

$$V_{OC} = \alpha(T_h - T_c) = \alpha\Delta T, \quad (1)$$

where T_c denotes temperature at cold-side, T_h denotes temperature at hot-side, α denotes Seebeck coefficient, and ΔT denotes the temperature difference between hot- and cold-sides.

The following Equations (2) and (3) show the energy balance used for steady-state analysis at hot- and cold-sides [34].

$$Q_h = \alpha I T_h - k_{tc}\Delta T - 0.5 I^2 R_{int}, \quad (2)$$

$$Q_c = \alpha I T_c - k_{tc}\Delta T + 0.5 I^2 R_{int} \quad (3)$$

where k_{tc} denotes the thermal coefficient of conductivity. The output power of the TEG can be expressed based on the above relations as follows Equation (4)

$$P_{teg} = Q_h - Q_c = \alpha(T_h - T_c)I - I^2 R_{int} = (\alpha\Delta T - IR_{int})I = V_{teg} I. \quad (4)$$

Referring to Figure 2, the TEG terminal voltage output (V_{teg}) can be given as Equation (5)

$$V_{teg} = V_{oc} - R_{int} I, \quad (5)$$

where R_{int} denotes the internal resistance of the TEG, and I denotes the TEG current.

According to the theory of maximum power transfer, the maximum available power can be achieved when the load resistance equals the internal resistance of TEG. The internal TEG resistance and TEG Seebeck coefficient can be formulated as Equations (6) and (7)

$$R_{int} = R_L = \frac{V_m^2}{P_m} \quad (6)$$

$$\alpha = \frac{2V_m}{\Delta T}. \quad (7)$$

2.2. Model Validation

To study the electrical characteristics of TEG (model TEG1-12611-6.0) under a standard temperature difference, the model of the TEG has been designed in MATLAB/Simulink software based on its thermoelectric properties discussed in the above section. Table 1 shows the electrical specifications of the TEG1-12611-6.0. Using the designed model, the electrical characteristics, namely Power vs. Voltage (P-V) and the current vs. voltage (I-V), are obtained and are shown in Figures 3 and 4. The results obtained from the designed model are compared with the manufacturing datasheet. From Figures 3 and 4, it can be confirmed that the designed model output is almost identical with the manufacture datasheet and confirmed the accuracy of the design.

Table 1. Specifications of TEG1-12611-6.0.

Characteristics	Specification
Cold-end temperature	30 °C
Hot-end temperature	300 °C
Open-circuit voltage	8.4 V
Matched load voltage	4.2 V
Matched load resistance	1.2 Ω
Matched load current	3.4 A
Matched load power	14.6 W

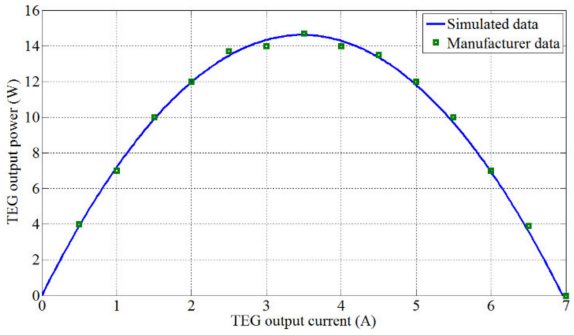

Figure 3. TEG1-12611-6.0 output power against the output current.

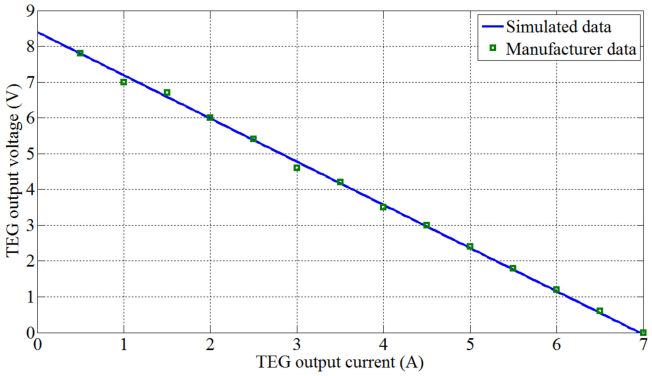

Figure 4. TEG1-12611-6.0 output voltage against the output current.

3. Incremental Resistance-Based MPPT Technique

The maximum power output from a TEG can be obtained by controlling the duty cycle of the DC-DC converter, which is part of the TEG system. The converter duty cycle modification is usually made by the maximum power point (MPP) tracking algorithm to harvest the maximum power based on the maximum power transfer theory [35,36]. The core idea of the incremental resistance technique is based on the derivative of power related to current (dP/dI) is zero at MPP as presented in Figure 5. More details about this technique can be found in [37]. The error signal e(t) can be derived as follows Equations (8) and (9)

$$\frac{dp}{dI} = \frac{d(V \times I)}{dI} = V + I\frac{dV}{dI} = 0, \tag{8}$$

$$\frac{dV}{dI} + \frac{V}{I} = \frac{V(t) - V(t-1)}{I(t) - I(t-1)} + \frac{V(t)}{I(t)} = 0.$$

Also,

$$e(t) = \frac{V(t) - V(t-1)}{I(t) - I(t-1)} + \frac{V(t)}{I(t)}. \tag{9}$$

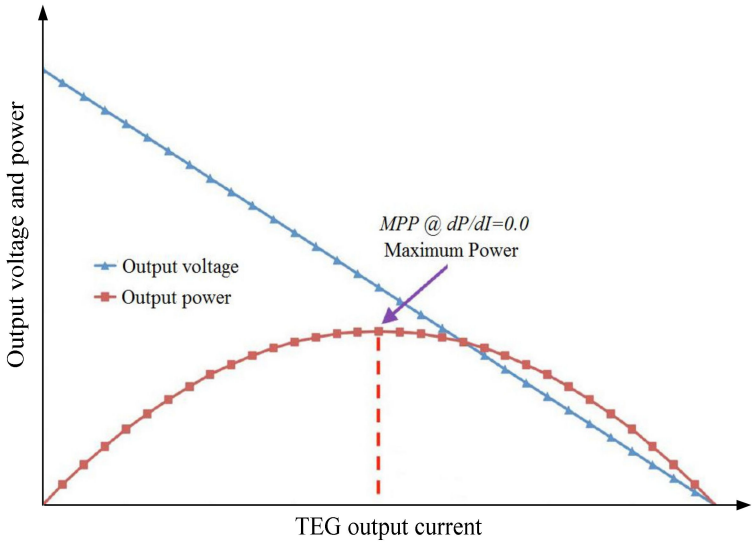

Figure 5. TEG electrical characteristics.

The error signal e(t) is very small around the maximum power point; therefore, to reduce the steady-state oscillations, the step size of the incremental resistance technique is selected based on the value of the error signal. To do this and model the incremental resistance technique, an integrator is used as illustrated in Figure 6. The integrator input is the error signal.

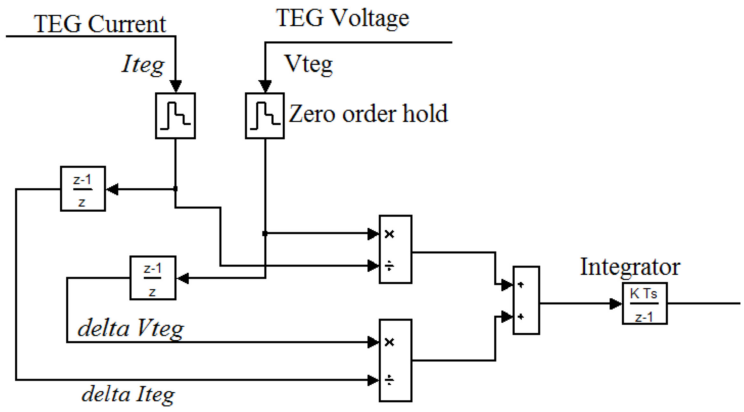

Figure 6. MATLAB model incremental resistance (INR) technique.

4. Variable Fractional Order Fuzzy Logic Controller-Based MPPT Technique

4.1. Fractional Order Control

In recent years, the fractional order calculus is used in various fields of science and engineering. The fractional order derivatives are commonly applied to enhance the controller performance in linear as well as nonlinear closed-loop systems. The fractional order control (FOC) method uses the principle of fractional calculus. Recently, many types of FOC methods have been proposed and investigated for different control applications. The FOC scheme consists of a non-integer order, which is preferred over the integer order control method due to its advantages [38]. When compared to integer-order control, the FOC provides more flexibility in design and exhibit better results in terms of robustness [39,40]. Based on the definition of Grunwald–Letnikov (GL) and Riemann–Liouville (RL) [41], the general expression for the fractional order differentiator (10) can be obtained. A detailed derivation of Equation (10) can be found in [42].

$$D_t^{\alpha} t^m \approx \frac{\Gamma(m+1)}{\Gamma(m+1-\alpha)} t^{m-\alpha}, \tag{10}$$

where α is the real number and it represents the order of derivative. The Gamma function $\Gamma(\alpha)$ can be defined as Equation (11)

$$\Gamma(\alpha) = \int_0^{\infty} e^{-t} t^{\alpha-1} dt. \tag{11}$$

The value of α is chosen as $0 < \alpha < 1$ and it characterizes the physical phenomenon of the system.

4.2. VFOFLC-Based MPPT Technique

The MPPT techniques are used to move the operating point of a generating system towards a peak level in the P-V curve to extract always the possible maximum power output from the source. To reach the peak level quickly corresponding to the MPP, a fractional factor α (alpha) is applied in the proposed MPPT technique, the factor α will expand or contract the domain of the VFOFLC input. Consider that if the input domain is expanded, then the VFOFLC will have a larger tracking step size to reach the MPP quickly. Based on the GL derivative equations, the derivative of power to voltage can be derived as Equation (12)

$$\frac{d^{\alpha} P}{dV^{\alpha}} = \lim_{\Delta V \to 0} \frac{1}{\Delta V^{\alpha}} \times \sum_{t=0}^{\infty} \frac{-1^t \Gamma(\alpha+1)}{\Gamma(t+1)\Gamma(\alpha-t+1)} P(V - t\Delta V), \tag{12}$$

where $\alpha > 0$, P (V − tΔV) is the power output of TEG at time *t*, and the corresponding terminal voltage is V. The power and voltage changes in TEG express the realistic approximations in fractional

order calculus. By approximating Equation (12), the changes in TEG power and voltage is expressed as Equation (13)

$$\frac{d^{\alpha}P}{dV^{\alpha}} \approx \lim_{\Delta V \to 0} \frac{P - \alpha P_0}{(V - V_0)^{\alpha}}, \tag{13}$$

where P and P_0 are the current and previous instant power, and V and V_0 are the current and previous instant voltage output of the TEG, respectively. Based on the fractional order calculus, the incremental change of the power is approximated as $d^{\alpha}P \approx P - \alpha P_0$ and the incremental change of the voltage is approximated as $dV^{\alpha} \approx (V - V_0)^{\alpha}$. The variations in power and voltage in unit time are taken as error e(t), the change in power in unit time is ΔP(t). The value of e(t) and ΔP(t) is calculated as follows Equations (14) and (15)

$$e(t) = \frac{P - P_0}{V - V_0}, \tag{14}$$

$$\Delta P(t) = P - P_0 \tag{15}$$

By considering the fractional order term, the Equation (14) can be modified as Equation (16)

$$e(t) = \frac{P - \alpha P_0}{(V - V_0)^{\alpha}}. \tag{16}$$

The value of the fractional factor α is $0 < \alpha \leq 1$, when α is $0 < \alpha < 1$, then the input domain of the VFOFLC will be modified based on α value. When $\alpha = 1$, the controller input domain is fixed, the method is just like a classical FLC-based MPPT technique; however, for the proposed MPPT algorithm, the domain of e(t) will be changed dynamically based on factor α of Equation (16). The smaller α will expand the input e(t), which leads to shortening the time to reach the MPP by increasing the tracking step size. When the MPP is approached, the bigger α will contract the input e(t) to attain a stable output around the MPP by reducing the tracking step size. In this paper, the factor α is determined based on the change in the voltages (ΔV) of the TEG in unit time ($\Delta V = V - V_0$). For example, if ΔV is zero then α will be 1, which indicates that the TEG operating point reaches MPP. Suppose that the MPP is not attained then ΔV is not equal to zero, the corresponding value of α will be between 0 and 0.9. Thus, the control logic is developed such that the smaller α can shorten the time of attaining the MPP. When the operating point is approaching near to the MPP then the value of α will be closer to 1. As compared to conventional incremental conduction (INC) tracker, the VFOFLC-based tracker will have a better steady-state and fast-tracking effect. The fast-tracking of MPP and a stable output around MPP will always minimize energy losses and improve the efficiency of the system.

5. Implementation of the VFOFLC-Based MPPT Technique

The block diagram for the proposed VFOFLC-based MPPT technique is illustrated in Figure 7, the power output of the TEG system is determined from the measured current (I) and voltage (V). The error e(t) and change in power ΔP(t) are computed based on Equations (15) and (16). The sign of e(t) indicates the current position of the TEG operating point in the P-V curve. For example, if e(t) is positive, the present operating point is left-side of the MPP, the negative value of e(t) indicates that the present operating point is right-side of MPP. Suppose that if e(t) is zero which confirms that the operating point reached MPP. Based on the error signal, the position of the operating point in the P-V curve can be determined, which is expressed in the following Equation (17)

$$e(t)\begin{cases} +ve;\ Left-side\ the\ MPP \\ \quad = 0;\ at\ the\ MPP \\ -ve;\ Right-side\ the\ MPP \end{cases} \tag{17}$$

Similarly, the sign of ΔP(t) determines the direction of the operating point movement. If e(t) is a negative and ΔP(t) is also negative, then the TEG voltage has to be decreased to attain the MPP.

Alternatively, if e(t) is negative but ΔP(t) is positive, which indicates that the TEG operating point is moving towards the MPP, hence, there is no need to change the TEG voltage. Suppose that if e(t) is positive and ΔP(t) is negative, then the TEG voltage has to be increased to attain the MPP. If e(t) is positive and ΔP(t) is also positive, which specifies that the operating point is moving towards the MPP, hence, there no need to change the TEG voltage. The voltage output of the TEG is changed by adjusting the duty cycle of the DC–DC boost converter.

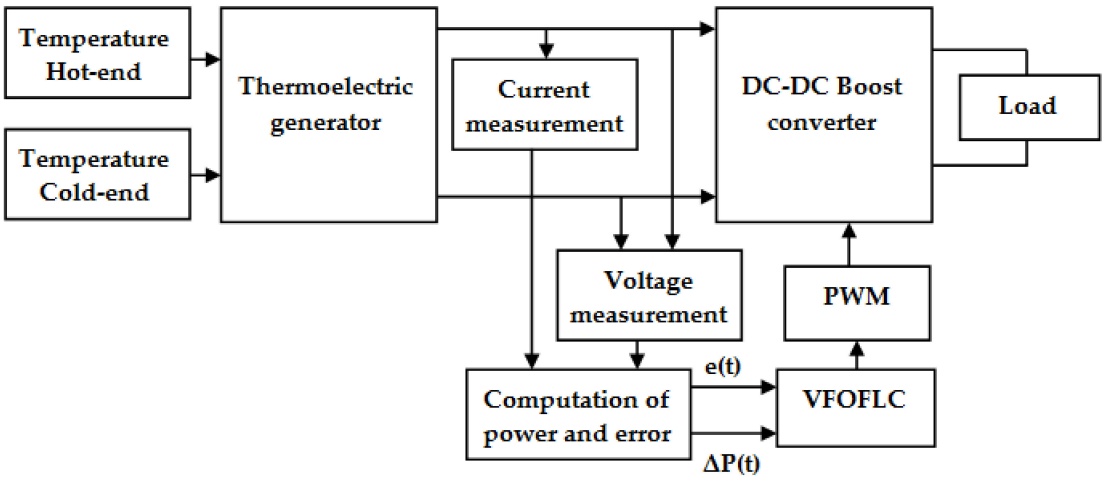

Figure 7. Block diagram of the variable fractional order fuzzy logic controller (VFOFLC)-based maximum power point tracking (MPPT) technique.

The control logic of the VFOFLC-based MPPT technique is illustrated in the flow chart shown in Figure 8. The type of power converter used to implement the MPPT is also being taken into consideration. Using error (16) and change in power (15), the VFOFLC controller block will generate an output u(t) with predefined fuzzy rules. A small u(t) will reduce the tracking step size to minimize the oscillations around MPP, the large u(t) will increase the tracking step size to move the TEG operating point quickly towards the MPP. The fuzzy logic controller (FLC) of the VFOFLC scheme is designed with five membership functions of triangular shape for the inputs as well as outputs. The linguistic term corresponding to the input membership functions are NB: Negative Big, NS: Negative Small, ZE: Zero, PS: Positive Small, and PB: Positive Big. Similarly, the linguistic term corresponding to output membership functions are represented as VS: Very Small, SM: Small, ME: Medium, HG: High, and VH: Very High. The membership functions of the inputs and output are shown in Figure 9. The fuzzy control rules are developed with the main objectives to quickly achieve the MPP and provide a stable output around MPP without much oscillation. The control rules are based on the control logic discussed previously in this section, for instance, if e(t) is NS or NB, then u(t) necessarily to be minimum (i.e., VS or SM) to decrease the output voltage, if e(t) is PS or PB then u(t) necessarily to be maximum (i.e., VG or HG) to increase the output voltage. Suppose, if e(t) is PB and ΔP(t) is PB or PS, then u(t) is VH. Once u(t) increases, the TEG output voltage also increases.

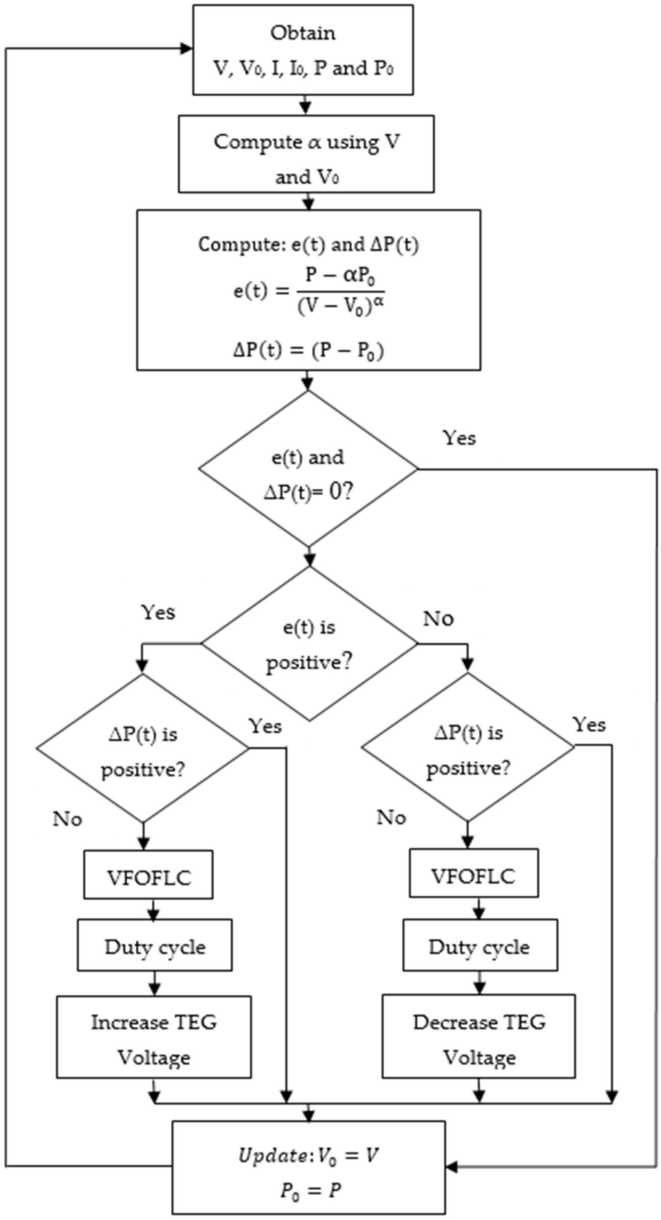

Figure 8. Control logic flow chart of the VFOFLC-based MPPT technique.

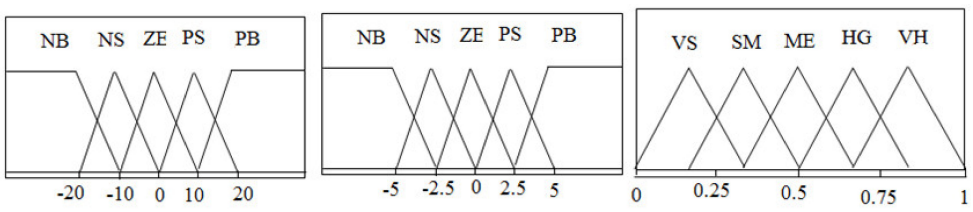

(**a**) (**b**) (**c**)

Figure 9. Membership function of the VFOFLC: (**a**) input error; (**b**) input change in power; (**c**) output duty cycle.

In the present system, twenty-five fuzzy control rules were developed in a similar fashion, which is shown in Table 2. The control rules represent the relationship between the input and output of the controller, the surface view of the fuzzy control rules used in the proposed system is shown in Figure 10. To examine the performance of the VFOFLC-based MPPT algorithm, the TEG system

includes a converter circuit is developed in MATLAB/Simulink environment. The circuit parameters of the continuous conduction current mode DC–DC boost converter are given in Table 3. Figure 11 shows the overall system model implemented in the MATLAB software.

Table 2. Control rules of the VFOFLC.

u(t)		e(t)				
		NB	**NS**	**ZE**	**PS**	**PB**
ΔP(t)	NB	VS	VS	SM	ME	HG
	NS	SM	SM	ME	ME	HG
	ZE	SM	ME	HG	HG	VH
	PS	ME	SM	SM	HG	VH
	PB	SM	HG	HG	VH	VH

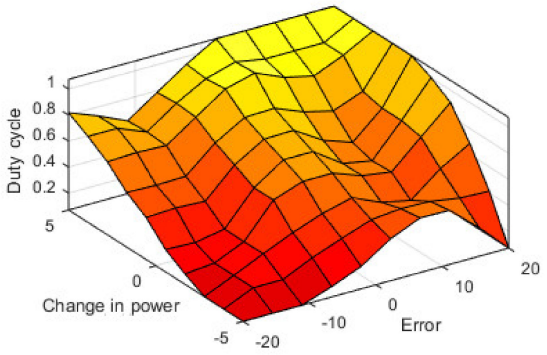

Figure 10. Surface view of the fuzzy control rules.

Table 3. Electrical parameters of the converter circuit.

Parameters	Values
Switching Frequency	25 kHz
Input Capacitor Cin	47 µF
Inductor, L	5 mH
Output Capacitor Cout	47 µF
Electrical load Resistance	25 ohms

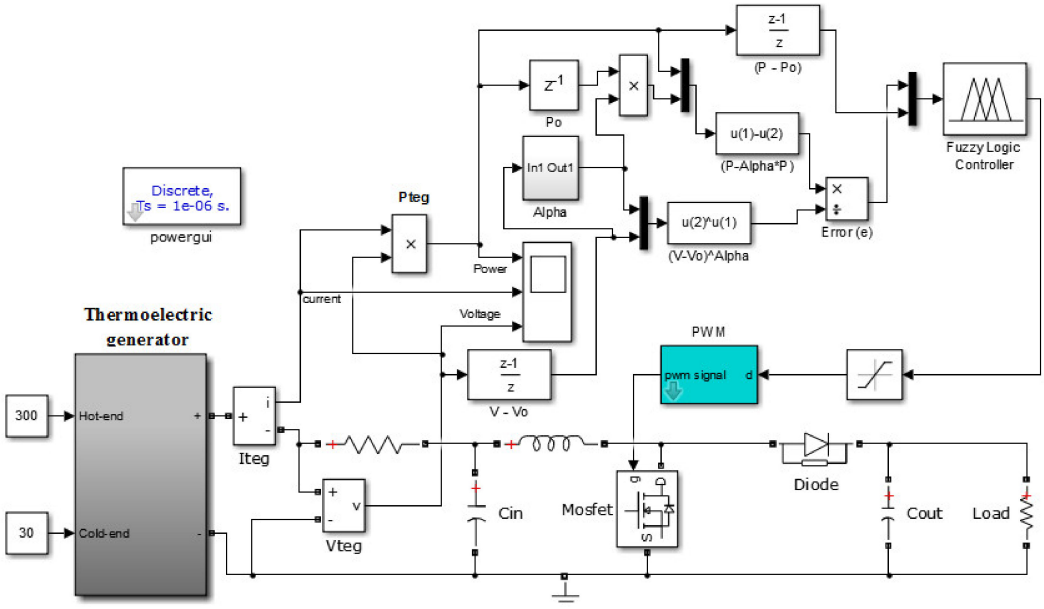

Figure 11. MATLAB-SIMULINK model of the VFOFLC-based MPPT technique.

6. Results and Discussion

To investigate the tracking performances of the designed VFOFLC- based MPP trackers, an extensive MATLAB simulation study under different thermal and electrical conditions was carried out. The results of the simulation studies are discussed in this section.

6.1. Fractional Factor and FLC Variable Discourse Range

The fractional factor, which is introduced in the VFOFLC-based MPPT scheme, changes the discourse range of the fuzzy input variable error e(t). Thus, the output parameters of TEG have a large change in the magnitude. The increase in the discourse of e(t) leads to shortening the time to reach the MPP. For example, when the fractional factor α is minimum, e(t) will be contracted, which leads to applying alternative control rules in the fuzzy logic system. The dynamic value of α is effective to reach the MPP quickly when there is a change in the load or variation in the temperature inputs. Reaching the MPP quickly and maintaining the operating point at the optimum level is necessary to improve the overall energy conversion efficiency. The fuzzy input e(t) discourse change is demonstrated with two different conditions (i.e., $\alpha = 1$ and $0 < \alpha < 1$), the variation in e(t) for these two conditions is illustrated in Figure 12. From Figure 12, if α is $0 < \alpha < 1$, the e(t) varies from +7 to −11 at the initial stage, and then gradually reaches approximately zero. This result clearly shows that e(t) will have a broad range at the beginning due to the variable fractional factor α. Suppose, if $\alpha = 1$ or it is not considered for the MPPT algorithm, the e(t) range is just only +7 to −5, which is the case of a classical FLC with fixed discourse. Thus, it is identified that the variation of α factor will be constructive for the dynamic domain range of the fuzzy input, which results in a better control action. A similar type of study, Tang et al. [42] proposed the fractional factor combined FLC to achieve the MPP for a photovoltaic system. In his study, the factor α will have a fixed value of either 0.1 or 0.5; however, in the proposed VFOFLC technique, the factor α will vary from 0 to 1 based on the output voltage variation in the TEG. Since the dynamic fuzzy domain variation can be achieved with α in the VFOFLC control scheme, which ensures the fast-tracking of MPP and a stable output around MPP.

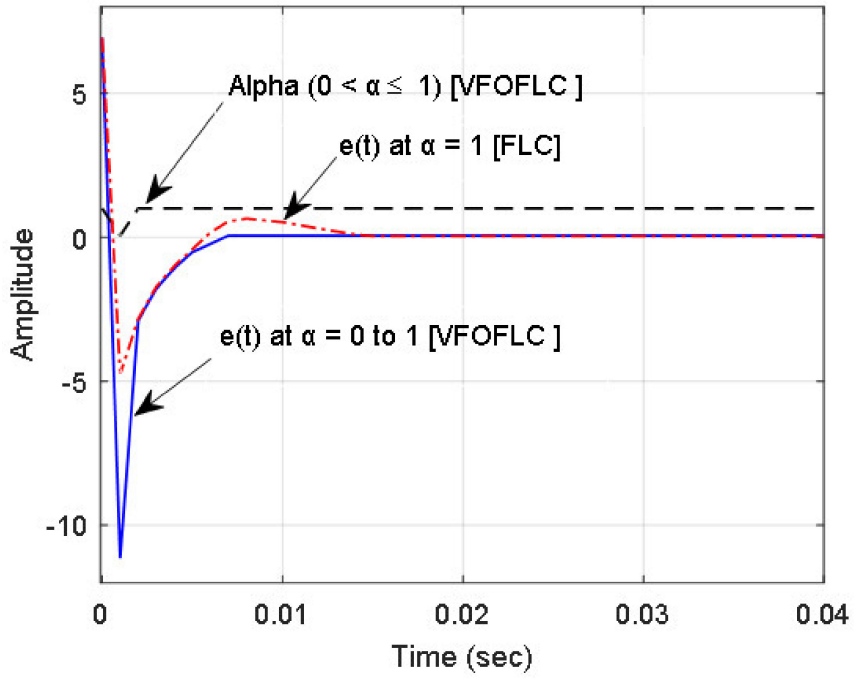

Figure 12. Variation in the domain range of the fuzzy input e(t) based on alpha.

6.2. TEG Performance for Load Variation

The electrical parameters of the TEG for different load conditions were studied to verify its energy conversion ability. The output response of the TEG with VFOFLC-based MPPT technique when the load resistance (R_L) is equal to 15, 20, and 25 ohms are shown in Figure 13. Figure 13a shows the power output of the TEG under different load conditions, the system provides nearly an equal power output for the different load. This result indicates that the proposed MPPT algorithm always maintains the MPP of the TEG even when there is a change in load. Since the DC–DC boost converter duty cycle is suitably adjusted, which results in the power at the load side is nearly a constant and maximum. The variation in the duty cycle for the different R_L is shown in Figure 13d, it is observed that the converter duty cycle is effectively modified based on the load. The voltage across the load and current flow for the different R_L is also depicted in Figure 13b,c which confirms the principle requirement of the voltage–current relationship of the equivalent DC circuit of the TEG represented in Figure 2. Similarly, the electrical outputs of the TEG using the INR-based MPPT algorithm were verified for the different load; the results of this study are shown in Figure 14. From these results, the power output of the TEG has more oscillation at the initial stage for a reasonable time. Further, it is seen that stable maximum power output is not achievable from the TEG immediately using this method. When compared to the VFOFLC-based MPPT technique, the INR-based MPPT technique, the maximum power output is not satisfactory for different load conditions. The other electrical parameters such as current, voltage, and the converter duty cycle for the INR-based MPPT technique were also examined for different loads as shown in Figure 14a–c. These parameters also have a similar kind of response at the initial period of the output.

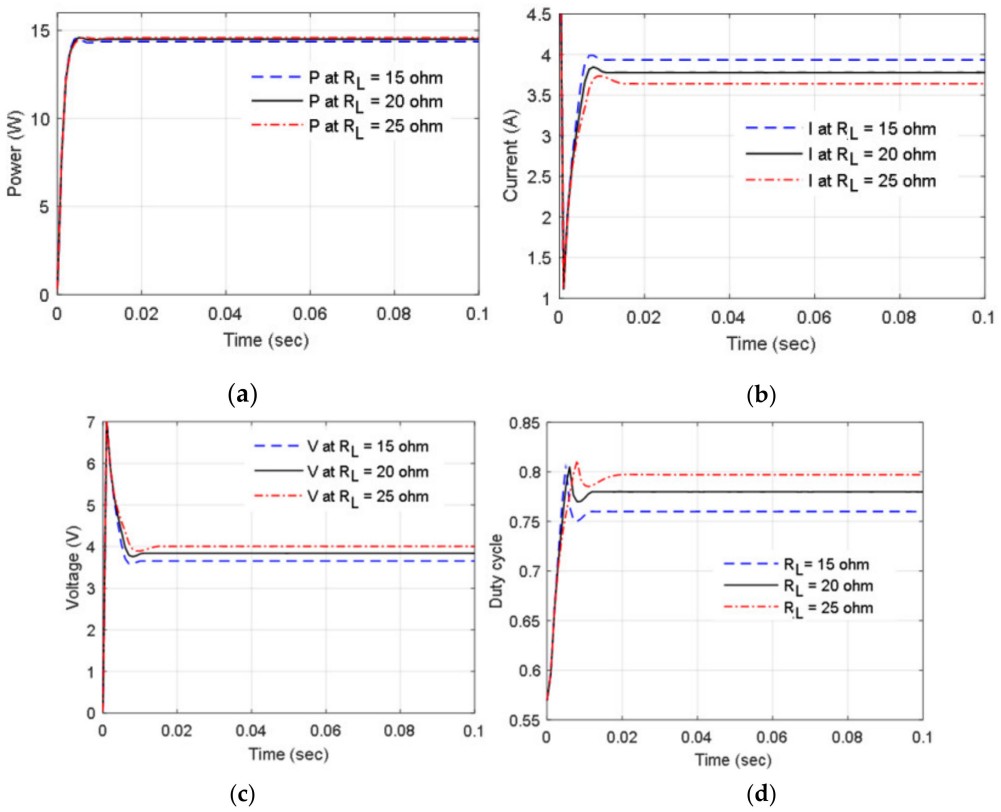

Figure 13. TEG performance using VFOFLC-based MPPT for the different load: (**a**) power output; (**b**) current flow; (**c**) voltage output; (**d**) duty cycle.

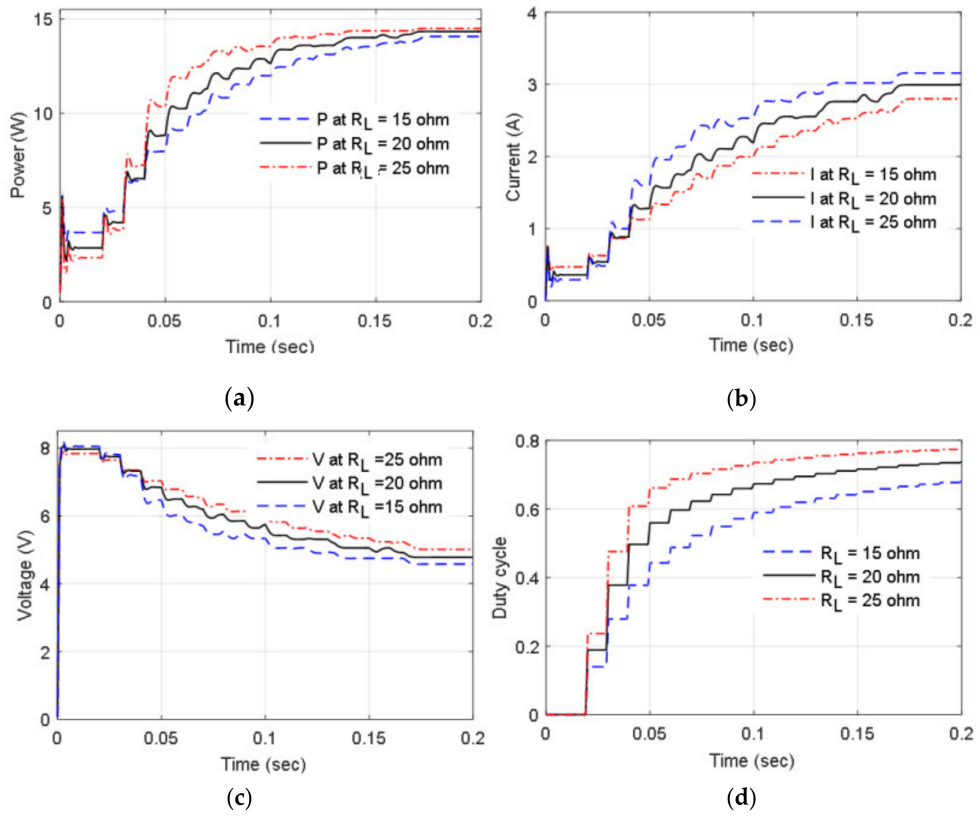

Figure 14. TEG performance using the INR-based MPPT for the different load: (**a**) power output; (**b**) current flow; (**c**) voltage output; (**d**) duty cycle.

6.3. TEG Performance for Step Changes in Temperature

The temperature difference applied across the inputs is considered to be an important factor that controls the electrical parameters of the TEG. Based on Equation (1), the open-circuit voltage (V_{OC}) of the TEG has a direct relation with the temperature difference across the hot- and cold-ends. The performances of the TEG using different MPPT control algorithms for the step-change in temperature difference are shown in Figure 15. Figure 15a represents the temperature difference applied at different time intervals; the corresponding electrical parameters such as power, voltage, and current using VFOFLC, P&O, and INR type MPPT techniques are depicted in Figure 15b–d. From Figure 15b, one can understand that the VFOFLC-based MPPT scheme identifies the changes in the temperature difference quickly and regulate the electrical output accurately without any delay and fluctuations. The TEG electrical parameters for the same temperature difference of Figure 15a using the P&O-based MPPT scheme is shown in Figure 15c. The results of Figure 15b,c are similar, but some moderate fluctuations are found at the initial period in the case of the P&O-based MPPT scheme of Figure 15c. The TEG performance using the INR-based MPPT scheme was also verified and the responses are illustrated in Figure 15d. The system output electrical parameters have more fluctuations at the initial period as well as when there is a change in the temperature difference. These comparison results demonstrate that the INR-based MPPT scheme is not advisable for the TEG system, where the input temperature difference will have frequent changes. Thus, the VFOFLC-based MPPT technique will be a better choice to obtain a steady-state output than the other two techniques.

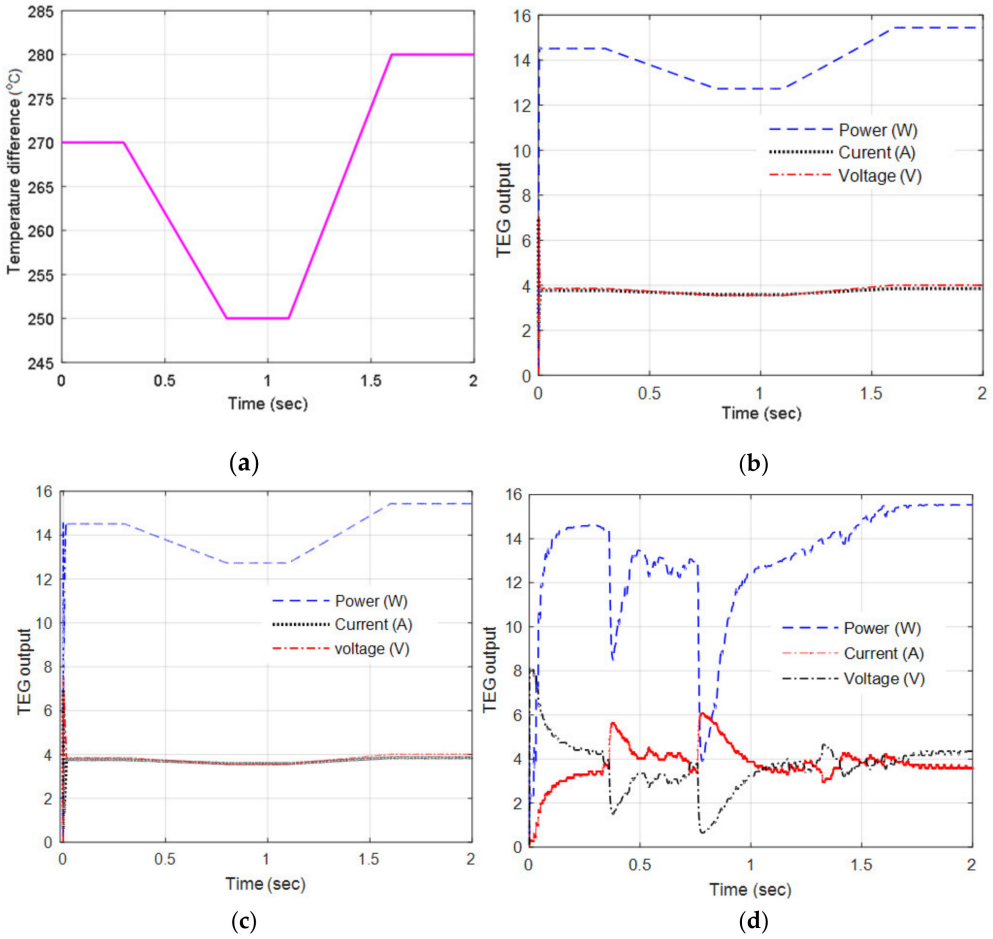

Figure 15. TEG performance for the change in temperature difference; (**a**) temperature difference applied at the input; (**b**) VFOFLC-based MPPT; (**c**) Perturb and observe (P&O)-based MPPT; (**d**) INR-based MPPT.

6.4. Performance Comparison for the Fixed Load and Temperature Difference

The effectiveness of the proposed tracker was verified by comparing its performance with INR and P&O type MPPT trackers for the fixed load and input temperature difference. For a fixed load of 25 ohms and an input temperature difference of 270 °C, the performance of the three MPPT trackers were tested and the results are shown in Figure 16. Figure 16a shows that the TEG output power using different MPPT trackers are nearly the same; however, in the case of the INR-based MPPT tracker, the TEG power output takes extra time to reach the final maximum value when compared to the other two types, since the INR-based MPP tracker is not capable of moving the operating point of the TEG at peak level quickly. On the other hand, the P&O type tracker shows a moderate performance, the output power of the TEG using this method has some fluctuations at the beginning, and in the final output level. The VFOFLC-based MPP tracker performance is better than the other two trackers at obtaining the maximum power promptly from the TEG without any fluctuations in the output. Thus, the proposed tracker can improve the efficiency and the overall performance of the TEG. Similarly, the voltage and current parameters are also compared for different MPPT techniques as shown in Figure 16b,c. These results demonstrate that the VFOFLC-based MPPT tracker is capable of providing a stable current and voltage unlike the INR and P&O types MPPT trackers. The duty cycle corresponding to this study for the three different MPPT techniques is shown in Figure 16d. From Figure 16d, it is noticed that the proposed MPPT technique generates an appropriate duty cycle from the initial period itself, which is essential to get a steady-state output. The INR-based MPPT technique the duty cycle has more oscillations at the initial period and takes additional time to reach a stable value. The VFOFLC-based MPPT technique effectively utilizes the fractional factor to set the

large tracking step size whenever the operating point of the TEG is not near to the MPP. Suppose that if the operating point of the TEG is around MPP, then the tracking step size is reduced via the fractional factor to avoid oscillations; therefore, the lively varying fractional factor and the variable tracking step size could enhance the maximum power harvesting performance of the VFOFLC-based MPPT technique; however, the computation of the fractional factor and the use of intelligent technique-based MPPT control algorithms may increase the complexity and computation time of the system.

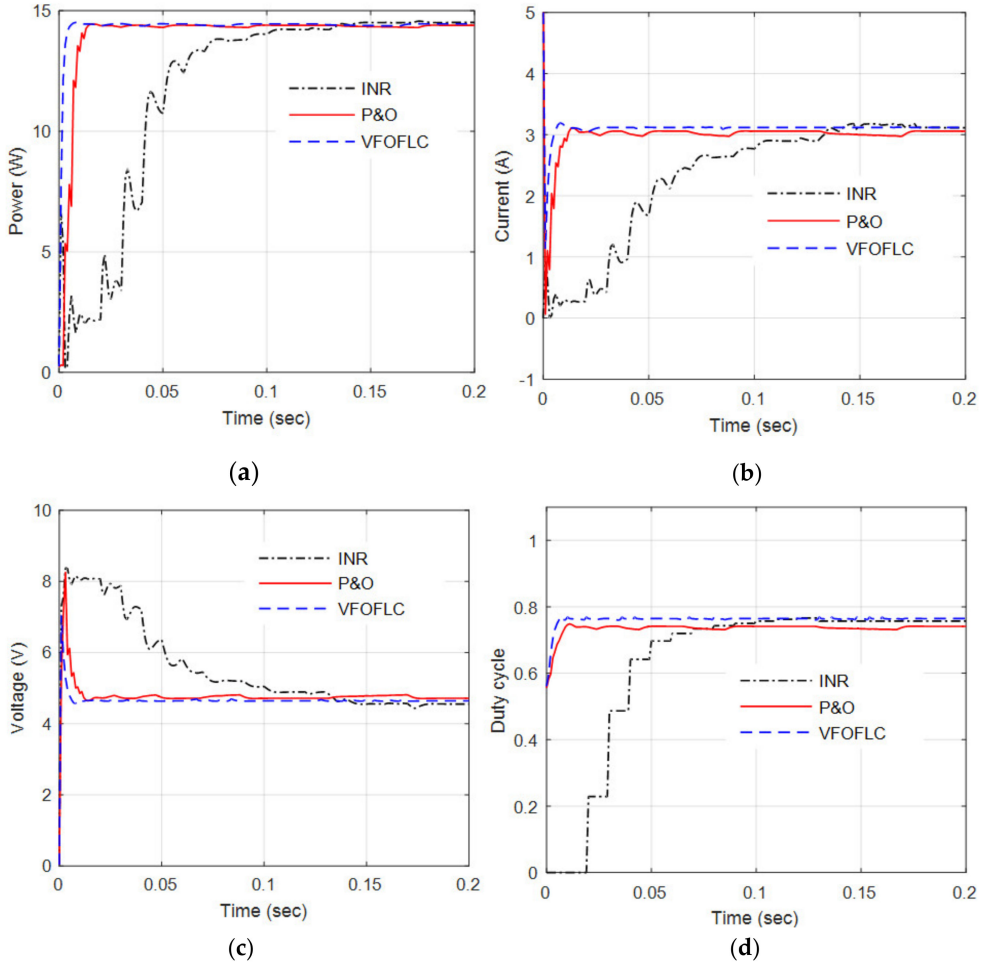

Figure 16. Performance comparison of different MPPT tracker: (**a**) power output; (**b**) current flow; (**c**) voltage output; (**d**) duty cycle.

The energy conversion efficiency of the TEG system has to always be high and stable to minimize energy losses. The conversion efficiency of the three different MPPT methods for the temperature difference of 300 and 250 °C was demonstrated as shown in Figure 17. The energy conversion efficiency is calculated based on the ratio of the electric output power to the temperature at hot-end (P/T_H). The comparison result of Figure 17 indicates that the proposed MPPT scheme is doing significantly better than the other methods. The VFOFLC-based MPPT scheme maintains the system efficiency at a stable level from the initial period, the efficiency of the system using INR-based MPPT scheme has more oscillations and takes a long time to reach a steady-state level. The energy conversion efficiency using the P&O-based MPPT technique also exhibits a moderate performance when compared to the INR-based MPPT scheme. Thus, the proposed VFOFLC-based MPPT scheme shows better performance in converting the thermal energy into electricity when compared to the other two MPPT schemes.

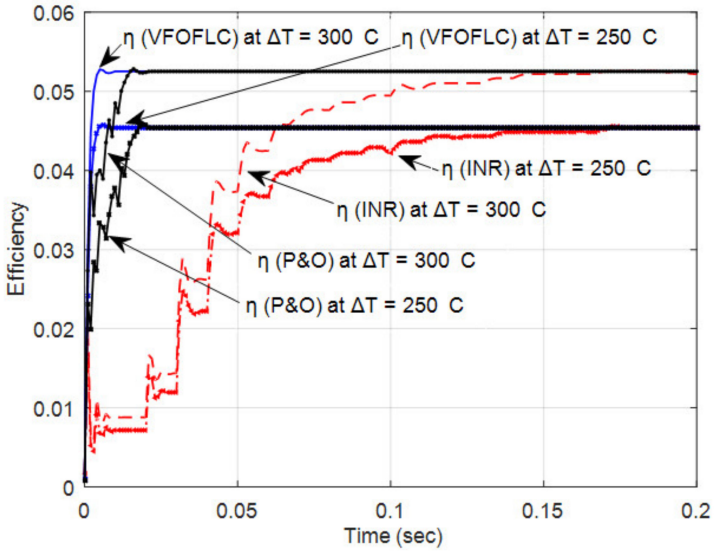

Figure 17. The conversion efficiency of the TEG.

7. Conclusions

In this paper, we present a novel VFOFLC-based MPPT technique to extract the maximum energy from the TEG. The fractional factor was introduced in the proposed MPPT technique to shorten the tracking time for reaching the peak level in the P-V curve and maintain steady-state output around MPP. The proposed MPPT technique was studied with a designed TEG model under both steady-state and transient conditions to demonstrate its effectiveness. The study results demonstrated that the VFOFLC-based MPPT technique has appropriately modified the duty cycle of the DC–DC boost converter using the variable fractional factor. Further, the present method guarantees the maximum energy extraction from the TEG over the wide range of load and temperature. The reduced tracking time, maximum and stable output power at MPP, and better energy conversion efficiency were achieved with the VFOFLC-based MPPT technique. Besides, the performance of the present MPPT technique has been compared with P&O and INR type MPPT techniques; the comparison results were confirmed, and show that the proposed method can efficiently harvest the maximum energy from the TEG even there was a change in temperature differences at the input and load variation conditions as well.

Author Contributions: Conceptualization, N.K. and H.R.; formal analysis, N.K. and H.R.; investigation, H.R. and M.R.G.B.; methodology, N.K. and H.R.; software, N.K. and H.R.; validation, H.R. and M.R.G.B.; writing—original draft preparation, N.K. and H.R.; writing—review and editing, H.R. and M.R.G.B. All authors have read and agreed to the published version of the manuscript.

Funding: This project was supported by the Deanship of Scientific Research at Prince Sattam Bin Abdulaziz University under the research project No. 2020/01/16817.

Conflicts of Interest: The authors declare no conflict of interest.

References

1. Twaha, S.; Zhu, J.; Yan, Y.; Li, B. A comprehensive review of thermoelectric technology: Materials, applications, modelling and performance improvement. *Renew. Sustain. Energy Rev.* **2016**, *65*, 698–726. [CrossRef]
2. Roy, A.; Klinefelter, A.; Yahya, F.B.; Chen, X.; Gonzalez-Guerrero, L.P.; Lukas, C.J.; Kamakshi, D.A.; Boley, J.; Craig, K.; Faisal, M.; et al. A 6.45 µW self-powered SoC with integrated energy harvesting power management and ULP asymmetric radios for portable biomedical systems. *IEEE Trans. Biomed. Circuits Syst.* **2015**, *9*, 862–874. [CrossRef] [PubMed]
3. Chen, J.; Klein, J.; Wu, Y.; Xing, S.; Flammang, R.; Heibel, M.; Zuo, L. A thermoelectric energy harvesting system for powering wireless sensors in nuclear power plants. *IEEE Trans. Nucl. Sci.* **2016**, *63*, 2738–2746. [CrossRef]

4. Charris, D.; Gomez, D.; Ortega, A.R.; Carmona, M.; Pardo, M. A thermoelectric energy harvesting scheme with passive cooling for outdoor IoT sensors. *Energies* **2020**, *13*, 2782. [CrossRef]
5. Dias, P.C.; Morais, F.J.O.; de Morais França, M.B.; Ferreira, E.C.; Cabot, A.; Dias, J.A.S. Autonomous multisensor system powered by a solar thermoelectric energy harvester with ultralow-power management circuit. *IEEE Trans. Instrum. Meas.* **2015**, *64*, 2918–2925. [CrossRef]
6. Montecucco, A.; Knox, A.R. Maximum power point tracking converter based on the open-circuit voltage method for thermoelectric generators. *IEEE Trans. Power Electron.* **2015**, *30*, 828–839. [CrossRef]
7. Yilbas, B.S.; Sahin, A.Z. Thermoelectric device and optimum external load parameter and slenderness ratio. *Energy* **2010**, *35*, 5380–5384. [CrossRef]
8. Lesage, F.J.; Pelletier, R.; Fournier, L.; Sempels, E. Optimal electrical load for peak power of a thermoelectric module with a solar electric application. *Energy Convers. Manag.* **2013**, *74*, 51–59. [CrossRef]
9. Kim, T.Y.; Negash, A.; Cho, G. Direct contact thermoelectric generator (DCTEG): A concept for removing the contact resistance between thermoelectric modules and heat source. *Energy Convers. Manag.* **2017**, *142*, 20–27. [CrossRef]
10. Selvan, K.V.; Mohamed Ali, M.S. Copper–Nickel and Copper–Cobalt thermoelectric generators: Power-Generating optimization through structural geometrics. *IEEE Trans. Electron Devices* **2018**, *65*, 3394–3400. [CrossRef]
11. Rezania, A.; Rosendahl, L.; Yin, H. Parametric optimization of thermoelectric elements footprint for maximum power generation. *J. Power Sources* **2014**, *255*, 151–156. [CrossRef]
12. Ibrahim, A.; Rahnamayan, S.; Martin, M.V.; Yilbas, B.S. Multi-Objective thermal analysis of a thermoelectric device: Influence of geometric features on device characteristics. *Energy* **2014**, *77*, 305–317. [CrossRef]
13. Jang, B.; Han, S.W.; Kim, S.W. Optimal design for micro-thermoelectric generators using finite element analysis. *Microelectron. Eng.* **2011**, *88*, 775–778. [CrossRef]
14. Selvan, K.V.; Rehman, T.; Saleh, T.M.; Ali, M.S. Copper-Cobalt thermoelectric generators: Power improvement through optimized thickness and sandwiched planar structure. *IEEE Trans. Electron Devices* **2019**, *66*, 3459–3465. [CrossRef]
15. Montecucco, A.; Knox, A. Accurate simulation of thermoelectric power generating systems. *Appl. Energy* **2014**, *118*, 166–172. [CrossRef]
16. Meng, J.H.; Zhang, X.X.; Wang, X.D. Dynamic response characteristics of thermoelectric generator predicted by a three-dimensional heat-electricity coupled model. *J. Power Sources* **2014**, *245*, 262–269. [CrossRef]
17. Chen, W.H.; Huang, S.R.; Wang, X.D.; Wu, P.H.; Lin, Y.L. Performance of a thermoelectric generator intensified by temperature oscillation. *Energy* **2017**, *133*, 257–269. [CrossRef]
18. Kim, R.; Lai, J.; York, B.; Koran, A. Analysis and design of maximum power point tracking scheme for thermoelectric battery energy storage system. *IEEE Trans. Ind. Electron* **2009**, *56*, 3709–3716.
19. Chandrarathna, S.C.; Lee, J. A dual-stage boost converter using two-dimensional adaptive input-sampling MPPT for thermoelectric energy harvesting. *IEEE Trans. Circuits Syst. I* **2019**, *66*, 4888–4900. [CrossRef]
20. Bond, M.; Park, J. Current-Sensorless power estimation and MPPT implementation for thermoelectric generators. *IEEE Trans. Ind. Electron.* **2015**, *62*, 5539–5548. [CrossRef]
21. Kim, J.; Kim, C. A DC–DC boost converter with variation-tolerant MPPT technique and efficient ZCS circuit for thermoelectric energy harvesting applications. *IEEE Trans. Power Electron.* **2013**, *28*, 3827–3833. [CrossRef]
22. Bijukumar, B.; Raam, A.G.K.; Ganesan, S.I.; Nagamani, C. A linear extrapolation-based MPPT algorithm for thermoelectric generators under dynamically varying temperature conditions. *IEEE Trans. Energy Convers.* **2018**, *33*, 1641–1649. [CrossRef]
23. Veerachacy, M.; Senjyu, T.; Uezato, K. Neural-Network-based maximum-power-point tracking of coupled-inductor interleaved-boost converter-supplied PV system using fuzzy controller. *IEEE Trans. Ind. Electron.* **2003**, *50*, 749–758. [CrossRef]
24. Rezk, H.; Eltamaly, A.M. A comprehensive comparison of different MPPT techniques for photovoltaic systems. *Sol. Energy* **2015**, *112*, 1–11. [CrossRef]
25. Ibrahim, H.E.; Houssiny, F.F. Microcomputer controlled buck regulator for maximum power point tracker for dc pumping system operates from photovoltaic system. In Proceedings of the IEEE International Fuzzy Systems Conference, Seoul, Korea, 22–25 August 1999; 1, pp. 406–411.
26. Tan, B.; Ke, X.; Tang, D.; Yin, S. Improved perturb and observation method based on support vector regression. *Energies* **2019**, *12*, 1151. [CrossRef]

27. Cheng, F.; Gao, Y.; Guo, X.; Yuan, X.; Fu, L.; Shi, L.; Han, X.; Zheng, K.; Wang, C.; Zhang, W. Fabrication of nanostructured skutterudite-based thermoelectric module and design of a maximum power point tracking system for the thermoelectric pile. *IEEE Sens. J.* **2019**, *19*, 5885–5894. [CrossRef]
28. Ahmed, E.M.; Shoyama, M. Stability study of variable step size incremental conductance/impedance MPPT for PV systems. In Proceedings of the 8th International Conference on Power Electronics—ECCE Asia, Jeju, Korea, 29 May–2 June 2011; pp. 386–392.
29. Kramer, L.R.; Maran, A.L.O.; de Souza, S.S.; Ando Junior, O.H. Analytical and numerical study for the determination of a thermoelectric generator's internal resistance. *Energies* **2019**, *12*, 3053. [CrossRef]
30. Xiao, W.; Dunford, W.G. A modified adaptive hill climbing MPPT method for photovoltaic power systems. In Proceedings of the 2004 IEEE 35th Annual Power Electronics Specialists Conference, Aachen, Germany, 20–25 June 2004; pp. 1957–1963.
31. Lineykin, S.; Ben-Yaakov, S. Modeling and analysis of thermoelectric modules. *IEEE Trans. Ind. Appl.* **2007**, *43*, 505–512. [CrossRef]
32. Tsai, H.; Lin, J. Model building and simulation of thermoelectric module using matlab/simulink. *J. Electron. Mater.* **2010**, *39*, 2105–2111. [CrossRef]
33. Laird, I.; Lu, D. High step-up DC/DC topology and MPPT algorithm for use with a thermoelectric generator. *IEEE Trans. Power Electron.* **2012**, *28*, 3147–3157. [CrossRef]
34. Yusop, A.M.; Mohamed, R.; Ayob, A.; Mohamed, A. Dynamic modeling and simulation of a thermoelectric-solar hybrid energy system using an inverse dynamic analysis input shaper. *Model. Simul. Eng.* **2014**, *2014*, 376781. [CrossRef]
35. Mohamed, M.A.; Diab, A.A.; Rezk, H. Partial shading mitigation of PV systems via different meta-heuristic techniques. *Renew. Energy* **2019**, *130*, 1159–1175. [CrossRef]
36. Abdalla, O.; Rezk, H.; Ahmed, E.M. Wind driven optimization algorithm based global MPPT for PV system under non-uniform solar irradiance. *Sol. Energy* **2019**, *180*, 429–444. [CrossRef]
37. Rezk, H.; Fathy, A. Performance improvement of PEM fuel cell using variable step-size incremental resistance MPPT technique. *Sustainability* **2020**, *12*, 5601. [CrossRef]
38. Kanagaraj, N. Design and performance evaluation of fuzzy variable fractional-order $[PI]^{\lambda}D^{\mu}$ controller for a class of first-order delay-time systems. *Stud. Inform. Control* **2019**, *28*, 443–452. [CrossRef]
39. Monje, C.A.; Chen, Y.Q.; Vinagre, B.M.; Xue, D.; Feliu-Batlle, V. *Fundamentals of Fractional-Order Systems*; Springer: London, UK, 2010.
40. Franklin, G.; Powell, J.; Naeini, A. *Feedback Control of Dynamic Systems*; Addison-Wesley: Boston, MA, USA, 1986.
41. Gutiérrez, R.E.; Rosário, J.M.; Machado, J.T. Fractional order calculus: Basic concepts and engineering applications. *Math. Probl. Eng.* **2010**, *2010*, 1–19. [CrossRef]
42. Tang, S.; Sun, Y.; Chen, Y.; Zhao, Y.; Yang, Y.; Szeto, W. An enhanced MPPT method combining fractional-order and fuzzy logic control. *IEEE J. Photovolt.* **2017**, *7*, 640–650. [CrossRef]